A Reliable Interference-Aware Mapping Algorithm for Airborne Tactical Network Virtualization

JINGCHENG MIAO, NA LV, KEFAN CHEN, WEITING GAO, AND YANHUI ZHANG
School of Information and Navigation, Air Force Engineering University, Xi'an 710077, China

Corresponding author: Na Lv (lvnn2007@163.com)

ABSTRACT Airborne tactical networks (ATNs) is driving the growing development of network-centric warfare by maintaining coverage and providing reach-back to military units. However, the key function of ATNs is impeded by the network ossification that is deep-rooted in the tightly coupled, vertically integrated architecture of traditional ATNs. Network virtualization (NV) can provide a more flexible and scalable ATN architecture as a solution, breaking the tight coupling between applications and network infrastructure. One important aspect of NV is virtual network embedding (VNE), which instantiates multiple virtual networks on a shared substrate network. However, existing efforts are not necessarily optimal for the virtualization of ATNs due to the absence of QoS-compliant capacity for the complex interference in air-combat field. To tackle this difficulty, a reliable interference-aware VNE algorithm, termed VNE-RIA, is proposed to provide reliable guarantee in the coordinated node and link mapping for various airborne tactical virtual networks (ATVNs). In the node mapping, the VNE-RIA adopts a novel node ranking approach to rank all substrate and virtual nodes, considering the complex interference including link interference, environmental noise and malicious attacks. In the link mapping, an improved anypath link mapping approach, based on the anypath routing scheme, is adopted to improve the reliability and efficiency of mapping virtual links by exploiting the unique features of wireless channels and the influence of different transmission rates. Numerical simulation results reveal that VNE-RIA algorithm outperforms typical and latest heuristic wireless VNE algorithms under the complex electromagnetic interference of ATNs.

INDEX TERMS Airborne tactical network, network-centric warfare, network virtualization, virtual network embedding, transmission rate.

I. INTRODUCTION

The revolution of network-centric warfare has been reshaping the current military communication infrastructure. In recent years, there is a significant push to rapidly deploy on-demand air resources such as blimps, unmanned aerial vehicles, and larger aircraft to construct airborne tactical networks (ATNs), which can maintain coverage and provide reach-back to military aircraft as well as surface and space military units [1]–[3]. However, current ATNs are application coupled with vertical integration of customized software stack and hardware, leading to insufficient interoperability and high

The associate editor coordinating the review of this manuscript and approving it for publication was Tachun Lin.

upgrading difficulty [4]. It also impedes the revolution of information communication technology (ICT) in the Internet of Battle Things [5]. Therefore, there exists a necessary need to effectively abstract network resources in order to support multi-mission multi-application in the developing ATNs.

With the ability of overcoming the resistance to architectural changes, network virtualization (NV) has been considered as a promising paradigm for many emerging areas like cloud computing [5] and smart IoT [6]. It enables multiple heterogeneous virtual networks (VNs) to coexist on the same substrate network (SN) and share underlying physical computing and networking resources simultaneously and seamlessly [7], [8]. Thus, NV can also provide a high level of resource sharing among various air-combat applications for

ATNs. Compared with the conventional NV methods, software defined networking (SDN) can offer direct global view of the usage state of network resources and strict QoS provisioning without tunneling overhead since it decouples control and data planes and flexibly offers end-to-end network slices according to the requirements of various applications [9]. Thus, it is able to provide a viable implementation platform for the virtualization of ATNs, called as airborne tactical network virtualization (ATNV).

Virtual network embedding (VNE) has been widely accepted as a vital step to implement NV [10]. It focuses on the effective embedding of VNs, with node and link resource demands (power, storage, bandwidth), onto the shared SN that has limited network resources [7]. Many great efforts have been made to propose heuristic algorithms in the solution of the VNE problem that has been proved to be NP-complete. These existing VNE schemes based on two-stage or one-stage mapping are mostly constructed for wired networks [11]–[14]. Thus, considering the negative influence of co-channel interference and noise, some VNE solutions have been proposed in the context of wireless networks [15]–[20], which focus on node mobility [17], [20], co-channel interference [18], fault tolerance [16] and QoS provisioning [15]. However, these wireless embedding algorithms cannot offer high-reliability guarantee for the ATNs with complex electromagnetic interference in the air-combat field.

The focus of this paper is on the design of reliable VNE techniques for ATNV considering the malicious attacks and vulnerable wireless channels in ATNs. Unlike general mobile wireless networks, ATNs are easily suffered from the techniques of electronic warfare including electronic jamming and electronic warfare destroying [4], which may invalidate the operations of virtual networks as the limited network resources are influenced. In such cases, VNE solutions shall take malicious attacks into consideration when mapping virtual nodes and links. In node mapping, the current greedy approach focuses on finding the most valuable substrate node by node ranking. However, traditional node-ranking approaches for wireless VNE algorithms [18] don't fully take the negative interference into account. It may lead to inefficient resource utilization in the long term, especially for ATNs with malicious attacks. In link mapping, the shortest-path or multi-commodity flow algorithm may not be necessarily optimal for ATNs with malicious attacks and vulnerable wireless channels. An anypath link mapping scheme was proposed in [15] to fulfill diverse QoS requests under the harsh industrial environment. However, the influence of different transmission rates is not fully explored under the harsh wireless interferences, which may increase the embedding cost in the long term.

In this paper, a reliable interference-aware mapping algorithm, termed VNE-RIA, is proposed to deal with VNE problem in a continuous time event for ATNs. The goals of VNE-RIA are to yield high embedding profits (minimal embedding costs) and high acceptance rate for ATNV in the harsh air-combat environment. Node mapping and link mapping are coordinated in the embedding process of virtual network request (VNR). When it comes to mapping a virtual node, a novel node-ranking approach is adopted to rank all substrate nodes and virtual nodes, according to the resources and topology attribute influenced by the harsh air-combat environment. As a virtual link is to be mapped, the improved anypath link mapping scheme is adopted in VNE-RIA, considering the influence of different transmission rates. To further validate the efficiency and reliability of VNE-RIA algorithm, a comprehensive simulation is also conducted in this paper. Numerical simulation results reveal that VNE-RIA algorithm performs better than representative and latest heuristic wireless VNE algorithms in terms of long-term average VNR acceptance ratio and average revenue to cost ratio in a continuous time event. These compared algorithms only consider the influence of wireless interferences on link mapping and adopt the shortest-path algorithm.

To recap, the main contributions of this paper are summarized as follows:

1) A novel node-ranking approach is proposed by considering the complex electromagnetic interferences that may affect the node ranking value of substrate nodes. The novel node-ranking approach is different from the previous universal node-ranking approaches for wireless VNE problem and ensures reliable resource utilization of SN in the long term.

2) A heuristic algorithm VNE-RIA, coordinating node mapping and link mapping, is proposed based on the novel node-ranking approach. When mapping a virtual link for ATNV, an improved anypath link mapping scheme is adopted by considering the influence of different transmission rates. Also, transmission rate can directly reflect the link propagation delay which is important for the delay sensitive air-combat missions in ATNs.

3) A comprehensive simulation is conducted to validate the efficiency and reliability of VNE-RIA algorithm. Typical and state-of-the-art wireless VNE algorithms, closely related to our VNE-RIA, are selected to make up the comparison. Simulation results clearly show that the VNE-TAGRD algorithm performs better than the existing wireless VNE algorithms for ATNs.

The remainder of our paper is organized as follows. Related work is introduced in Section II. Section III formulates the VNE problem and proposes the SDN based virtualization model for ATNs. Then, the details of VNE-RIA algorithm are presented in Section IV. The simulation work is implemented in Section V, along with specific simulation parameters setting. Finally, Section VI concludes this paper and puts forward the prospects of future work.

II. RLATED WORK

The current ATNs are actually based on discrete data link systems (e.g. Link-11, Link-16, TTNT), which follow the chimney-style, designed in a stacked and one-stop manner, to satisfy specific tactical communications demands. Although they manage to provide necessary communications for command and guidance, situational awareness, and

primary tactical coordination [4], the vertically integrated network architecture has been formed, leading to a lack of flexibility, interoperability, and evolvability for the evolution of ATNs. Moreover, the issue of ATNs also exists in many public networks, especially for unmanned aerial vehicles (UAVs) networks. As a promising network paradigm, NV has been a recent research focus area within the aviation field [21].

VNE has been accepted as one key aspect in the implementation of NV. Recent surveys [10], [22] present a detailed classification of relevant VNE algorithms. VNE aims to optimally map virtual nodes and links into the same shared SN as various VNRs arrive in a discrete or continuous time event. VNE problem can be formulated as a graph isomorphism that is known to be NP-hard [23]. Therefore, many efforts have been made in the heuristic approaches, which compromise global optimality for a relatively short execution time. Based on these backgrounds, this section only discusses heuristic VNE algorithms that are closely related to VNE-RIA algorithm.

A. TIPICAL AND WIRED HEURISTIC ALGORITHMS
In the past years, most of the typical heuristic algorithms have been proposed for wired networks. The embedding of each given VN can be conducted in two stages: 1) node mapping stage and 2) link mapping stage. Therefore, these VNE algorithms can be divided into two-stage (separated node and link mapping) and one-stage (coordinated node and link mapping) heuristic algorithms. One-stage algorithms have a relatively higher time complexity but perform better in the embedding revenue of VNRs.

In the node mapping stage, the current greedy approach focuses on ranking all the substrate nodes and virtual nodes and finding the most valuable nodes [24]. The node ranking value includes topology attribute (e.g. node degree or node strength) and local network resources (e.g., the nodes capacity resources or the product of nodes capacity resources and their adjacent link bandwidths). Recently, references [14], [25] explored global resources that focused on the resource influence between nodes and utilized multiple topology attributes simultaneously. Cao *et al.* [14] proposed a heuristic VNE algorithm considering the network topology attribute and network resource. It mapped virtual nodes by a node ranking approach simulated from Google PageRank website algorithm, calculating the stable node ranking value of nodes from five important network topology attributes and global network resources. Efficient node mapping approach needs to consider all the key information for calculating the node ranking value of both substrate nodes and virtual nodes. Otherwise, the resource fragmentation may be caused, which is unfeasible for accepting VNRs with large sizes. Therefore, for wireless networks, it is quite necessary to take the influence of link interferences (main challenge for wireless VNE) into account in node mapping stage.

In the link mapping stage, most existing heuristic algorithms adopt the shortest path algorithm or multicommodity flow approach [26]. For mapping a virtual link, the link requirements (e.g. bandwidth, propagation delay, transmission rate) must be satisfied. These link mapping approaches may lead to a high blocking of VN and make insufficient use of network resources. Thus, authors in [27] propose to allow the VN to split a virtual link over multiple substrate paths on the shared SN, solving the multi-commodity flow problem. However, these approaches are designed for wired links that possess relatively stable communication quality. To solve the wireless link mapping problem, one of the key aspects is to deal with the link interference when mapping a virtual link into the corresponding reliable wireless substrate path.

B. REPRESENTATIVE AND WIRELESS HEURISTIC ALGORITHMS
Recently, wireless network virtualization has gained more attention [7]. Designing wireless VNE algorithms needs to take network dynamics (e.g. wireless link quality instability, links failure, node mobility) into consideration. In this paper, we consider the wireless link quality instability that are mainly caused by link interference, environmental noise and malicious attacks.

Lv *et al.* in [19] proposed an enhanced genetic algorithm based VNE approach on static wireless mesh networks (WMNs). This approach mainly designed OFDMA-based WMN architecture, called as IGW-trees, to avoid co-channel interference between neighbouring nodes for virtual access network embedding. The node ranking approach only considered throughput information constraint, which may cause resource fragmentation and inefficient substrate utilization in the long term. And the link mapping adopted an enhanced genetic algorithm with the initial input generated by the shortest path algorithm. Also, Kaiwartya *et al.* in [16] proposed a VNE framework in wireless sensor networks (WSNs), adopting a genetic algorithm based link mapping approach. However, the framework lacks a full consideration of node mapping, not to mention the influence of link interference on node ranking.

Yun *et al.* in [18] proposed another heuristic algorithm for wireless VNE. The main highlight of [18] was the definition of influence weight assigned to substrate wireless links to quantify link interference. The node ranking value of nodes was the product of node capacity resources and their adjacent link bandwidth, ignoring the influence of link interference. The link mapping stage adopted the shortest path algorithm in terms of interference weight, which may not be optimal for wireless VNE since unique features of wireless channels are not fully exploited. In addition, Cao *et al.* in [28], simulating from [18], proposed a wireless VNE algorithm based on joint bandwidth and power allocation. This embedding algorithm utilized transmission rate to cooperate the bandwidth and power resources for load balancing. However, the node ranking approach ignored the influence of link instability and link mapping approach adopted the shortest path algorithm which may be not optimal for wireless VNE problem.

Li *et al.* in [29] proposed an application-driven virtual network embedding scheme to facilitate the QoS provisioning for wireless industrial networks. The scheme AVNE employed an anypath link mapping approach based on the anypath routing scheme, utilizing the broadcast nature of wireless channels. However, the node ranking value of nodes was only determined by packet loss rate, which may not fully exploit the other important node information like node capacity resources. In addition, the anypath link mapping lacked consideration of the influence of different transmission rates on the anypath routing scheme. The influence is important for the fast transmission of tactical information in ATNs.

C. BRIEF SUMMARY OF PREVIOUS WORKS

To summarize, NV can provide a promising solution to the ossification problem of ATNs. As a key aspect of NV, the VNE problem (which is known to be NP complete) needs to be further studied in the virtualization of ATNs. VNE algorithms are mostly heuristic and designed for wired networks (*subsection A*) to efficiently map virtual nodes and links into the SN. For wireless VNE problem (*subsection B*), one of the main challenges is the wireless link quality instability caused by link interference, environment noise and malicious attacks. However, current wireless VNE algorithms are not well suitable for ATNs since the influence of link interference on node ranking is not fully considered in node mapping. And link mapping approaches tend to adopt the shortest path algorithm which may not be proper for the unreliable quality of wireless links, especially in air-combat field. Therefore, despite the great efforts of related wireless VNE algorithms, it is still important to fully consider the influence of link quality instability on both node mapping and link mapping, especially for ATNs with complex electromagnetic interference in air-combat field.

The VNE-RIA algorithm, proposed in this paper, differs from previous wireless heuristic algorithms in four main aspects. First of all, the algorithm adopts a novel node ranking approach to rank all substrate nodes and virtual nodes, considering the influence of link quality instability mainly caused by link interference, environmental noise and malicious attacks. Second, the VNE-RIA utilizes the improved anypath link mapping approach to reliably map a virtual link with specific transmission rate onto the substrate path. Next, the node and link mapping are coordinated to achieve a better performance in embedding each ATVN request. Finally, a comprehensive simulation is implemented against typical heuristic algorithms under changing interference.

III. NETWORK MODEL AND PROBLEM FORMULATION

This section presents the virtualization for ATNs, including ATNV model, substrate network and ATVN (request) models, ATVN embedding stages and main evaluation metrics.

A. SLICE-BASED VIRTUALIZATION FOR ATN

In the traditional ATNs, manned and unmanned military aircrafts, as well as surface and ground platforms, form a
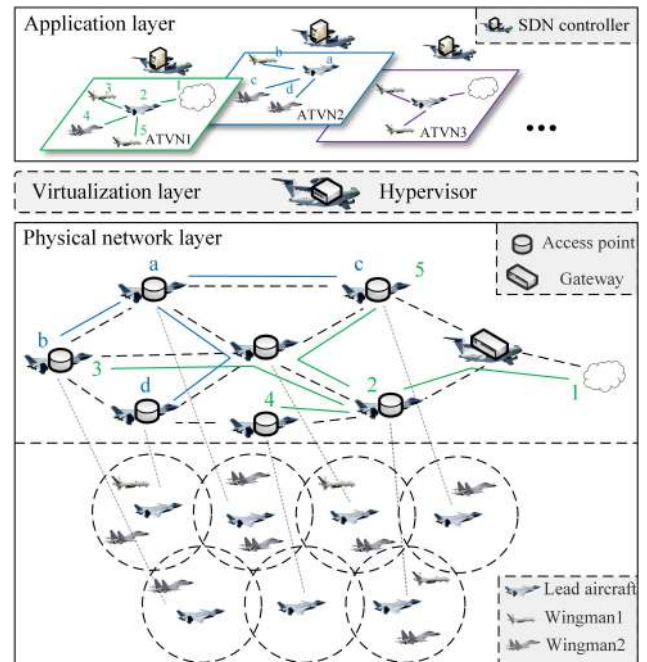

FIGURE 1. Illustration of slice-based virtualization for ATN.

large-scale wireless multi-hop network with tightly coupled and vertically implemented architecture to support users and applications. In view of the ossification problem, it is really essential to construct a more scalable and flexible infrastructure to effectively implement virtualization for ATN, which can be based on the SND-enabled ATN in [30] and inspired by the virtualization scheme in [15].

As shown in Fig. 1, a sliced virtualization scheme, designed for ATNs, is composed of the following three layers:

1) Physical network layer. Massive manned or unmanned aircrafts are deployed in concomitant formation to perform military missions. In the formation, the lead aircrafts with SDN-enabled devices, viewed as access points, compose the data plane for accessing and transferring military information, which forms a large-scale wireless multi-hop network that is abstracted as the shared airborne tactical substrate network (ATSN).

2) Virtualization layer. The hypervisor controls the ATSN and performs as a slicing agent between the data plane and control plane (which is composed of SDN controllers). Also, it can orchestrate and collaborate multiple applications in an overlapped way.

3) Application layer. Military mission services are transformed into multiple logical and self-contained airborne tactical virtual networks (ATVNs) with arbitrary topologies and customized QoS demands. Each ATVN has a dedicated SDN controller to directly support the protocol evolution.

Fig. 1 illustrates three applications in ATNs with strict transmission rate request. For instance, in the aerial reconnaissance mission, an ATVN can be distributed reconnaissance aircrafts, where sensors collaboratively monitor the situation information of the air-combat field in real time.

The situation information can be used for both operational decision under strict timing constraints and data collection for further military airborne missions.

In general, this virtualized ATN possesses four main features. First of all, it can make various network services flexibly coupled with military airborne missions, which may solve the ossification problem of current ATNs [7]. Second, heterogeneous ATNs can be coordinated seamlessly since each ATVN is allowed to run its own protocol. Next, the network configuration in one ATVN is isolated from that in another, which can efficiently and securely satisfy the dynamically changing communication demand of military missions [31]. Finally, it does not need to deploy extra devices for the developing innovative military applications, which can considerably decrease the overhead. Thus, new network technologies can be deployed quickly and easily due to the scalability and sustainability [8].

B. VNE PROBLEM MODEL

The ATSN can be abstracted and modeled as an undirected graph $G^S = (N^S, L^S)$, where N^S is the set of nodes served as access points for lead aircrafts and L^S is the set of wireless links, respectively. Each substrate node $n \in N^S$ is associated with a current radio transmission power p^S, a specific location $loc(n)$. The transmission capability p^S includes basic power $p_b(n)$ (which is used within the aviation formation) and remaining power $p(n)$ (which is used between aviation formations). In addition, the location $loc(n)$ is assumed to be unchanged and defined by x and y coordinates in this paper. In the aviation formation, each wingman can communicate with the lead aircraft within its transmission range. With respect to each substrate link $l^S \in L^S$, $b(l^S)$ denotes the finite bandwidth resource and $loc(l^S)$ denotes the relative location of the link. P^S denotes the set of all loop-free substrate paths. $P^S(n_i, n_j)$ is the set of all loop-free paths that connect substrate nodes n_i and n_j. $p^S(n_i, n_j)$ is one substrate path selected from the set $P^S(n_i, n_j)$. The down part of Fig. 2 presents the airborne tactical substrate network. The numbers beside the substrate nodes denote available radio transmission power $p(n)$. Also, numbers over the links denote available link bandwidth $b(l^S)$.

An ATVN is represented as an undirected graph $G^V = (N^V, L^V)$, where N^V is the set of all virtual nodes and L^V is the set of all virtual links. For each virtual node $v \in N^V$, R_N^V denotes the required node capability and $loc(v)$ denotes the location of the aircraft (lead aircraft or wingman) where the remote command and control platform wants to transmit tactical information and collect situation data. The coverage radius of v is denoted by φ^V. Substrate nodes, served as mapping candidates for n^V, must be within φ^V. For each virtual link $l^V \in L^V$, it has the required transmission rate $R(l^V)$ since the military missions tend to require that tactical information must be transmitted as fast as possible, which is closely related to the transmission rate that wireless links can offer. The up part of Fig. 2 shows an airborne tactical virtual
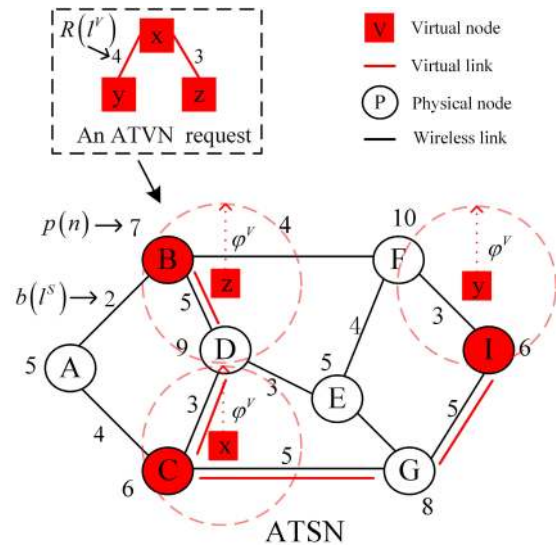

FIGURE 2. An embedding example of one ATVN request.

network with specific topology. The numbers over the links denote the required transmission rate $R(l^V)$.

C. EMBEDDING PROCESS

In general, the embedding of each ATVN request mainly includes two stages: the stage dealing with the mapping of virtual nodes, and the stage ensuring the mapping of virtual links. An ATVN embedding example is clearly shown in the following Fig. 2.

1) NODE MAPPING STAGE

To each ATVN request, different virtual nodes are not allowed to be mapped onto the same substrate node, which improves the flexibility and manageability of the ATSN. The assignments of all virtual nodes of one ATVN request can be represented as the node mapping function $M^N(N^V) : v \in N^V \to M^N(v)$

$$M^N(v) \in N^S$$
$$M^N(v_i) = M^N(v_j), \quad \text{iff } v_i = v_j$$

subject to

$$R_N^V \le R_N^S \tag{1}$$

$$Dist\left(loc\left(M^N(v)\right), \quad loc(v)\right) \le \varphi^V \tag{2}$$

where (1) aims to ensure that the required node capability of virtual node v, represented as R_N^V, must not exceed the offered node capability of the selected substrate node $M^N(v)$, represented as R_N^S; (2) aims to ensure that the selected substrate node must be within the required radius φ^V. R_N^S can be related to the available node transmission capability of substrate nodes. Both two formulas must be satisfied simultaneously in the node mapping stage. As shown in Fig. 2, the node mapping results of virtual nodes of an ATVN request are $M^N(x) = C$, $M^N(y) = I$, and $M^N(z) = B$.

2) LINK MAPPING STAGE

In this paper, for each virtual link of the ATVN request, a single reliable substrate path is selected after corresponding end nodes (virtual nodes) are mapped into the substrate nodes. Formally, the link mapping can be presented as $M^L(L^V)$: $l^V = (v_i, v_j) \in L^V \rightarrow M^L(l^V)$ for each virtual link of the ATVN request

$$M^N(l^V) \subseteq P^S\left(M^N(v_i), M^N(v_j)\right)$$

subject to

$$R(l^V) \leq R_L^S\left(p^S\left(M^N(v_i), M^N(v_j)\right)\right) \tag{3}$$

where (3) aims to ensure the transmission rate requirement of any virtual link l^V must not exceed the remaining transmission rate capability of one selected substrate path. This formula must be satisfied in the beginning of the link mapping stage. As shown in Fig. 2, for the virtual links of one ATVN request, the link mapping results are $M((x, y)) = \{(C, G), (G, I)\}$ and $M((x, z)) = \{(C, D), (D, B)\}$.

The embedding of any ATVN request fails if the demands of both node mapping stage and link mapping stage cannot be simultaneously completed. Then, the ATVN request gets to be rejected. To improve the understanding, the embedding process of one ATVN request is illustrated in Fig. 3.
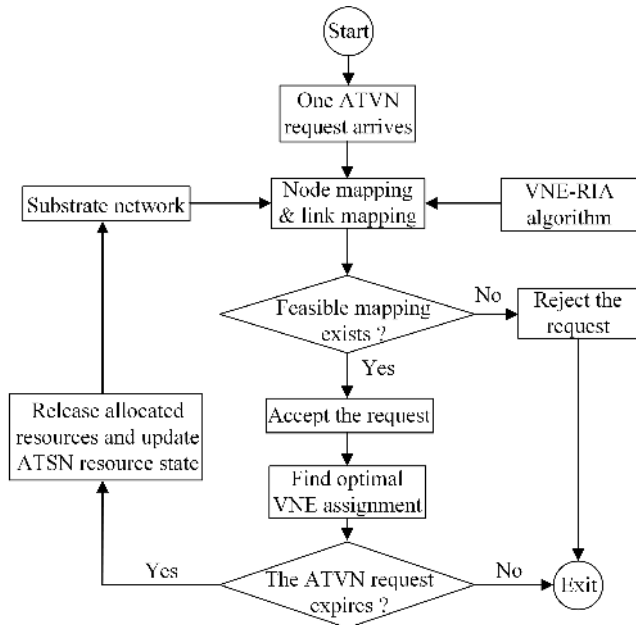

FIGURE 3. The embedding process of one ATVN request.

D. VNE DESIGN EVALUATION METRICS

In this paper, the objective is to develop a reliable VNE algorithm that finds feasible embeddings while maximizing the embedding profit and considering the complex electromagnetic interference in ATNs. In this subsection, two main evaluation metrics are formulated to quantify the advantages of the proposed VNE-RIA algorithm. Other metrics

(node power utilization, link bandwidth utilization, etc.) have been formulated well in [10].

The average acceptance ratio is an important metric in the VNE research. It is shown in (4) below.

$$\eta_{suc} = \lim_{T \to \infty} \frac{\sum_{t=0}^{T} NUM_{Emb}(t)}{\sum_{t=0}^{T} NUM_v(t) + \delta} \tag{4}$$

where $NUM_{Emb}(t)$ denotes the number of successfully embedded ATVN requests at time t. $NUM_v(t)$ denotes the total number of ATVN requests at time t. δ denotes a constant which is infinitely close to zero.

The long-term average revenue to cost ratio is another important performance metric of VNE algorithms. It is shown in (5) below.

$$R/C = \lim_{T \to Te} \frac{\sum_{t=0}^{T} \sum_{G_V \in VN_{map}(t)} R(G_V, t)}{\sum_{t=0}^{T} \sum_{G_V \in VN_{map}(t)} C(G_V, t)} \tag{5}$$

where $VN_{map}(t)$ denotes the running ATVN requests at time t. The revenue $R(G^V, t)$ and cost $C(G^V, t)$ are expressed as follows:

$$C(G^V, t) = \alpha \sum_{v \in N^V} p(n)|_{v \to n} + \sum_{l^V \in L^V} \sum_{l^S \in p^S} b(l^S)|_{l^V \to p^S} \tag{6}$$

$$R(G^V, t) = \beta \sum_{v \in N^V} p(n)|_{v \to n} + \sum_{l^V \in L^V} \sum_{l^S \in p^S} \frac{b(l^S)|_{l^V \to p^S}}{|p^S|} \tag{7}$$

where α and β denote weighting coefficients that coordinate the relationship between the node power resources and link bandwidth resources, respectively. Without loss of generality, both α and β are assumed to be 1, indicating that the importance of the power and bandwidth resource is similar. Also, $p(n)|_{v \to n}$ denotes the power resource allocated by the selected substrate node n for mapping virtual node v. If virtual link l^V is mapped onto the substrate path p^S, $b(l^S)|_{l^V \to p^S}$ denotes the bandwidth resource allocated by the wireless link l^S of the path p^S for mapping virtual link l^V. $|p^S|$ denotes the total number of wireless links of the substrate path p^S.

IV. VNE-RIA ALGORITHM

This section describes the proposed VNE-RIA algorithm in detail. At first, a novel reliable node ranking approach is presented, considering the complex interference in air-combat field. And the greedy node mapping is implemented based on the novel node-ranking approach. Next, an improved anypath link mapping scheme is adopted by considering the influence of different transmission rates on the link reliability. In the last section, the node mapping and link mapping are coordinated in one stage. In addition, the time complexity of VNE-RIA is

also presented to prove that VNE-RIA algorithm can conduct the embedding of each given ATVN request in polynomial time.

A. NOVEL RELIABLE NODE RANKING APPROACH

This subsection clearly presents the novel node ranking approach that is adopted in node mapping for the VNE-RIA algorithm. In a traditional node ranking approach, all substrate nodes and virtual nodes are ranked before implementing the embedding of arrived VN request. Then, two sorted node lists are formed and based on the node ranking value that indicates the embedding capacity of corresponding nodes. The virtual node with the highest node ranking value will be always mapped onto the substrate node that ranks highest in the substrate node list. Therefore, it is quite important to construct the node ranking value, considering the specific wireless environment of ATNs for the embedding of ATNV. The node ranking value also needs to estimate the transmission capability of corresponding substrate nodes since the key request of ATNV is to transmit the important military situation information as fast as possible.

For the arrived ATVN request $G^V = (N^V, L^V)$, the mapping of one selected virtual node v can be represented as $M^N(v) : v \rightarrow n$. For all virtual nodes in the set N^v, the node ranking value can be expressed as

$$NoV(v) = \sum_{l^V \in L_n^V} R\left(l^V\right) \tag{8}$$

where L_n^V denotes the set of virtual links that use virtual node v as one of their end nodes. Then, $NoV(v)$ reflects the total requirement of transmission rate for the corresponding virtual links of virtual node v.

In the substrate network $G^S = (N^S, L^S)$, the node ranking value of selected substrate node n is shown as

$$NoV(n) = \sum_{l^S \in L_n^S} R(l^S, t) \tag{9}$$

with

$$R(l^S, t) = b(l^S, t)lb\left(1 + \frac{p(n, t) g(l^S)}{AveInf(n) + AveInf(l^S)}\right) \tag{10}$$

where (9) presents the ability of substrate node n^S to provide high enough transmission rate for the ATVN request. For the selected substrate node n, L_n^S is the set of substrate links that use n as one of their end nodes and $R(l^S, t)$ denotes the highest transmission rate that the substrate link l^S can offer. In addition, (10) expresses a more specific mathematic explanation of $R(l^S, t)$ according to the famous *Shannon formula*. In (10), $p(n, t)$ denotes the remaining power resource of substrate node n at time t. For the corresponding link l^S in the L_n^S, $b(l^S, t)$ denotes the remaining bandwidth resource of substrate link l^S at time t and $g(l^S)$ denotes the link gain. Also, $AveInf(n)$ denotes the average node interference that is shown as

$$AveInf(n) = \frac{p_b(n)}{p_{Noise}(n) + p_{Attack}(n)} \tag{11}$$

Here, $p_{Noise}(n)$ represents the estimated effective power of environmental noise and $p_{Attack}(n)$ denotes the estimated effective power of malicious attacks. $p_{Attack}(n)$ is assumed to be the most unstable interference cause. This is the first attempt to describe the degree of interference to substrate nodes in literature [10].

The average link interference, disturbing the normal communication of link l^S, is denoted by $AveInf(n^S)$ that is represented as

$$AveInf\left(l^S\right) = \sum_{l_i \subset L^S \setminus l^S} Dist\left(l^S, l_i\right) p(n_i, t) g(l_i) \tag{12}$$

$$Dist\left(l_i, l^S\right) = \begin{cases} 2\eta, & \text{if } Dlink \leq Dhop \\ \eta, & \text{if } Dhop < Dlink \leq 2Dhop \\ \delta, & \text{if } Dlink > 2Dhop \end{cases} \tag{13}$$

In (12), $g(l_i)$ denotes the link gain of any other substrate link l_i in the set L^S. $p(n_i, t)$ denotes the available node power resource on the substrate link l_i. $Dist(l^S, l_i)$ denotes the distance coefficient between l_i and l_i. In (13), $Dhop$ denotes the average *Euclidean Distance* between two substrate nodes. Also, the *Euclidean Distance* between l_i and l_i is denoted by $Dlink = dist\{loc(l_i), loc(l^S)\}$. In addition, η is a constant and δ denotes a constant which is infinitely close to zero.

According to the node capacity constraint (1), the node ranking values of both the selected substrate node n and virtual node v need to meet the requirement that is expressed as

$$\frac{NoV(n)}{|L_n^S|} \geq \frac{NoV(v)}{|L_n^V|} \tag{14}$$

where $|L_n^S|$ and $|L_n^V|$ denotes the number of elements in the set L_n^S and L_n^V, respectively. The procedures of novel reliable node ranking approach are shown in **Algorithm 1** below.

As for the time complexity, let $|N^S|$ and $|N^V|$ denote the total number of substrate nodes and virtual nodes, respectively. Thus, the inner loop (step 6 to 8) of **Algorithm 1** requires at most $O(|N^S|^2)$ steps since there are at most $O(|N^S|)$ substrate links that link a substrate node. Therefore, the worst case time complexity of **Algorithm 1** is $O(|N^V||N^S|^2)$.

B. IMPROVED ANYPATH LINK MAPPING SCHEME

In view of the complex electromagnetic interference of ATNs, traditional wired link mapping approaches, based on the shortest-path or multicommodity flow algorithm, may not be optimal to map virtual links of the ATVN request. In addition, the ATVN request has a strict demand on transmission rate. Therefore, an improved anypath link mapping scheme, considering the transmission rate, is adopted for embedding ATVN request in this subsection.

For the arrived ATVN request $G^V = (N^V, L^V)$, the mapping of one selected virtual link l^V can be expressed as $M^N(l^V) : l^V \rightarrow p^S \in P^S$. The design of an improved anypath link mapping is based on the opportunistic routing [32], where one selected node receives and transmits the message

---

Algorithm 1 Node Ranking

Input: The arrived ATVN request $G^V = (N^V, L^V)$, substrate network $G^S = (N^S, L^S)$
Output: The *NoV* (v) with corresponding *NoV* (n)
1. **for** each selected virtual node v **do**
2.   **for** all the virtual links in the set L_n^V **do**
3.   Calculate the node ranking value of v as in (8) and get *NoV* (v);
4.   **end for**
5.   **for** each substrate node n that meets (2) **do**
6.   **for** each l^S that belongs to L_n^S **do**
7.   Calculate $R(l^S, t)$ according to (10);
8.   **end for**
9.   Calculate the node ranking value of n as shown in (9) and get *NoV* (n);
10.   **end for**
11.   Ignore the substrate nodes that cannot meet the node capacity requirement (14);
12.   **if** there are not proper substrate nodes that meet (14) **do**
13.   Reject the ATVN request;
14.   **end if**
15. **end for**

---

that will be forwarded by one of its adjacent nodes with different priorities. The transmitting and forwarding process can be described as a hyperlink, which is composed of a transmitter $n \in N^S$ and a set of forwarding adjacent nodes $\Gamma_n \in N^S$. For the selected virtual link l^V, the mapped anypath p^S can be described as its node set $\Phi(p^S)$ with the corresponding forwarding set $\Gamma_n, n \in \Phi(p^S)$. For each forwarding substrate link l^S in a hyperlink (n, Γ_n), its successful delivery probability can be estimated by

$$p_{nm} = \gamma \frac{R(l^S, t)}{R(l_{\max}^S, t)}, \quad m \in \Gamma_n \qquad (15)$$

where γ denotes the normalized constant and $R(l_{\max}^S, t)$ denotes that the max transmission rate that substrate links can possess at time t. Then, the successful delivery probability of a hyperlink can be expressed as

$$p_{n\Gamma_n} = 1 - \prod_{m \in \Gamma_n} (1 - p_{nm}) \qquad (16)$$

To map a virtual link through anypath routing, the expected anypath transmission time (EATT) is adopted as a metric for each node $n \in N^S$ to evaluate the anypath cost, which can be recursively calculated as

$$d_{n\Gamma_n} = \frac{1}{p_{n\Gamma_n}} \times \frac{B}{R(l^V)} \qquad (17)$$

$$D_n = d_{n\Gamma_n} + D_{\Gamma_n} \qquad (18)$$

where $d_{n\Gamma_n}$ denotes the hyperlink EATT from n to Γ_n and B denotes the link bandwidth of the selected link. In (18), D_{Γ_n} is the EATT of the remaining-anypath. It is defined as a weighted average of the EATTs of all adjacent nodes in Γ_n, which is presented as

$$D_{\Gamma_n} = \sum_{m \in \Gamma_n} w_m D_m \qquad (19)$$

where w_m denotes the weight that means the probability of node m being the relaying node. Let $\Gamma_n = \{1, 2, \cdots, M\}$ with the EATTs $D_1 \leq D_2 \leq \cdots \leq D_M$. Thus, w_m can be expressed as

$$w_m = \frac{p_{nm} \prod_{k=1}^{m-1} (1 - p_{nk})}{1 - \prod_{m \in \Gamma_n} (1 - p_{nm})} \qquad (20)$$

According to (17) and (18), a reliable path p^S with less transmission time can be found for any virtual link l^V that is selected to be mapped onto the SN. Also, to improve the long-term embedding revenue, it is important to properly allocate the path resource (node power and link bandwidth resource) for load balancing [28]. In this paper, the transmission rate is also utilized to allocate the path resource. For one substrate link l_i on the path p^S, its mapping cost for the path resource can be expressed as

$$C_i = \xi \frac{\Delta p_i}{p(n_i, t)} + \frac{\Delta b_i}{b(l_i, t)} \qquad (21)$$

where ξ denotes the weighting coefficient. $p(n_i, t)$ denotes the available node power resource on the link l_i and $b(l_i, t)$ denotes the available link bandwidth. Δp_i and Δb_i are variables that respectively denote the node power and link bandwidth resource that is going to be occupied. According to (10), the relationship between Δp_i and Δb_i can be expressed as

$$R(l^V) = \Delta b_i lb \left(1 + \frac{\Delta p_i g(l_i)}{\sigma^2 + AveInf(l_i)} \right) \qquad (22)$$

where σ^2 denotes the effective power of channel noise that can be estimated as

$$\sigma^2 = \frac{\omega}{2} \sum_{m \in \{n_i^1, n_i^2\}} p^b(m) \Big/ AveInf(m) \qquad (23)$$

where ω denotes a constant and $\{n_i^1, n_i^2\}$ denotes the set of corresponding end nodes of the link l_i.

As can be seen from (22), there exists a trade-off between Δp_i and Δb_i, which means the increase in Δp_i will cause the decrease in Δb_i. Therefore, (21) and (22) are combined can be combined to minimize the mapping cost C_i, which is presented as

$$C_i = \xi \frac{\Delta p_i}{p(n_i, t)} + \frac{R(l^V)}{b(l_i, t) lb \left(1 + \frac{\Delta p_i g(l_i)}{\sigma^2 + AveInf(l_i)} \right)} \qquad (24)$$

In (24), the mapping cost function is a concave function. Thus, the minimal C_i can be achieved with proper Δp_i and corresponding Δb_i.

The improved anypath linking mapping scheme is detailed in **Algorithm 2**. We extract the current substrate node m with

the minimum anypath cost, using the function EXTRACT-MAX(Q). In addition, the worst case time complexity of *Algorithm 2* is $O(|N^S|\log(|N^S|) + |L^S|)$ [32], in which $|L^S|$ denotes the total number of substrate links.

Algorithm 2 Link Mapping
***
Input: Substrate network $G^S = (N^S, L^S)$, one selected virtual link l^V, transmission rate $R(l^V)$, corresponding mapped substrate nodes n_{src} and n_{dst};
Output: The mapped p^S for the selected virtual link l^V;
1. **for** each substrate node $n \in N^S$ **do**
2. $D(n) \leftarrow \infty; F(n) \leftarrow \emptyset$;
3. **end**
4. $D(n_{dst}) \leftarrow 0; Q \leftarrow N^S; S \leftarrow \emptyset$;
5. **while** $Q \neq \emptyset$ and $n_{src} \notin S$ **do**
6. $m \leftarrow$ EXTRACT-MIN(Q);
7. $S \leftarrow S \cup \{m\}$;
8.   **for** each link l^S_{nm} and $R(l^S_{nm}, t) \geq R(l^V)$ **do**
9. $J \leftarrow F(n) \cup \{m\}$;
9.   **if** $D(n) > D(m)$ **then**
10. $D(n) \leftarrow d_{nJ} + D(J); F(n) \leftarrow J$;
11.   **end if**
12.   **end for**
13. **end while**
14. Collect p^S from n_{src} recursively via BFS (Bread First Search);
15. **if** p^S does not exist **do**
16.   Reject the arrived ATVN request;
17. **end if**
18. Calculate the Δp_i and Δb_i of link l_i on the p^S according to (23).

C. MAPPING IN ONE STAGE

There is a lack of heuristic one-stage algorithms since previous one-stage algorithms are mostly based on optimization theory and graph theory, involving much more VN assignment calculation time [33]. Therefore, we coordinate the node mapping (which adopts the ranking approach in *Algorithm 1*) and link mapping (which is shown in *Algorithm 2*) to improve the long-term revenue of embedding the arrived ATVN requests. And, the VNE-RIA algorithm, a heuristic one-stage embedding scheme, is proposed in *Algorithm 3* for embedding the ATVN requests.

In *Algorithm 3*, we extract the current substrate m with the highest node ranking value, using the function EXTRACT-MAX (V). The substrate node n with highest node ranking value is extracted by the function EXTRACT-MAX (Q). *Li* denotes the set of virtual links that link current virtual node n to virtual nodes that have been mapped. The function EXTRACT-MAX (Li) is used to extract the current virtual link l^V with the highest transmission rate request.

The time complexity of *Algorithm 3* is mainly determined by the node mapping (step 2 to 5) and link mapping (step 6 to 14). The time complexity of node mapping is determined by

---

Algorithm 3 Mapping in One Stage
***
Input: Substrate network $G^S = (N^S, L^S)$, an arrived ATVN request $G^V = (N^V, L^V)$;
Output: Results of the ATVN request embedding;
1. $V \leftarrow N^V; Q \leftarrow N^S; M \leftarrow \emptyset$;
2. **while** $V \neq \emptyset$ **do**
3.   Run *Algorithm 1*;
4. $m \leftarrow$ EXTRACT-MAX(V);
5. $n \leftarrow$ EXTRACT-MAX(Q);
6.   Map m onto n; $M \leftarrow M \cup \{m\}$; $Li \leftarrow \emptyset$
7.   **for** each virtual node $k \in M$ **do**
8.   **if** the virtual link $l^V_{mk} \in L^V$ exists **do**
9. $Li \leftarrow Li \cup \{l^V_{mk}\}$;
10.   **end if**
11.   **end for**
12.   **while** $Li \neq \emptyset$ **do**
13. $l^V \leftarrow$ EXTRACT-MAX(Li);
14. $n_{src} \leftarrow$ End node with smaller *AveInf(n)*;
15. $n_{dst} \leftarrow$ End node with bigger *AveInf(n)*;
16.   Run *Algorithm 2*;
17.   **end while**
18. **end while**
19. Update the residual link and nodal resources.

---

step 2. Therefore, the worst case complexity is $O(|N^V||N^S|^2)$. In addition, the worst case complexity of link mapping is $O(|N^V||L^V| + |L^V|(|N^S|\log(|N^S|) + |L^S|))$, in which $|L^V|$ denotes the total number of virtual links. Therefore, the total time complexity of *Algorithm 3* can be described as $O(|N^V|(|N^V||N^S|^2 + |N^V||L^V| + |L^V|(|N^S|\log(|N^S|) + |L^S|)))$.

V. SIMULATION EVALUATION

In this section, simulation results are given to illustrate our proposed VNE-RIA algorithm for the virtualization of ATNs. At first, the simulation parameter settings are presented in the form of tables. Next, main simulation results are illustrated. Thus, to quantify the advantage of VNE-RIA proposed in this paper, two comparative experiments are established. In the first simulation experiment, the performance of the VNE-RIA is compared with three algorithms under general interference. In the second simulation experiment, we simulate and illustrate the performance of the VNE-RIA under changing interference.

A. SIMULATION SETTING AND PARAMETERS

In this paper, the ATSN and ATVN topology are generated by the improved Salam network topology random generation algorithm [13]. The network parameters of the shared ATSN and ATVN are summarized in Table 1 and Table 2, respectively.

For the ATSN, we assume that all the substrate nodes have the basic power $p_b(n) = 10^{-4}$ and environmental noise power $p_{Noise}(n) = 10^{-6}$. The substrate link gain is

TABLE 1. Atsn parameters.

Parameter	Description
Scope	$200km \times 200km$
Number of substrate nodes	50
Number of substrate links	139
Available node power between flight formation	[50, 100], uniform distributed
Link bandwidth	[20, 50], uniform distributed

TABLE 2. Atvn parameters.

Parameter	Description
Number of virtual nodes	[3, 5], uniform distributed
Link connection probability	0.5
Link transmission rate	[3, 8], uniform distributed
VNR arrival rate	5 per 100 time units, Poisson process
VNR lifetime	100 time units

TABLE 3. Compared algorithms.

Notation	Description
G-SP [27]	The node ranking approach is based on the node capacity and the link mapping approach is the shortest path algorithm.
VNE-JBP [28]	The node ranking approach is based on the joint node power and link bandwidth and the link mapping approach is multipath link mapping.
VNE-RIAs	The node ranking approach is based on the node ranking value in (10) and the link mapping approach is multipath link mapping.
VNE-RIA	The node ranking approach is based on the node ranking value in (10) and the link mapping approach is the improved anypath routing link mapping.

$G = d^{-k}$, where d denotes the *Euclidean Distance* between corresponding end nodes and the channel fading coefficient is $k = 4$. For the ATVN, the coverage radius of one virtual node is set to be $\varphi^V = 100km$.

Simulations run for about 20000 time units. η in (13) is set to be 0.2. γ, ξ and ω in (15), (21) and (23) are all set to be 1. All simulations for different VNE algorithms are run on a Window 10 Laptop, with an Intel R Core (TM) CPU i7-7700@2.8GHz Processor and 8.00G RAM Machine. The analysis software is MATLAB R2019b.

B. COMPARED ALGORITHMS

As listed in Table 3, the simulation is made up of four heuristic wireless VNE algorithms using the same ATSN and ATVN requests.

All the other three algorithms are typical and latest to the proposed VNE-RIA algorithm with respect to node mapping and link mapping. They are also all slightly modified to fit into the simulation. Taking the modified G-SP algorithm as an

example, we clarify the criteria for whether the ATVN request is successful accepted. For any virtual link, link mapping finds the shortest path and calculates the transmission rate that the path can hold. If it is less than the transmission rate of corresponding virtual link, the ATVN request will be rejected.

C. SIMULATION RESULTS

In this subsection, we compare the simulation results of the VNE-RIA algorithm with the other three listed heuristic embedding algorithms under general and changing interference, respectively. For the general interference, it is assumed that there are not much malicious attacks in the air-combat field. Then, the general interference is expressed as $AveInf(n) = 1$, which is also equal to $0dB$ ($S/N = 10\lg(AveInf(n))$). Next, the changing interference are also expressed as $AveInf(n)$, which changes from $-12dB$ to $4dB$. The malicious attacks are set to get worse as the $AveInf(n)$ decreases.

1) COMPARISION UNDER GENERAL INTERFERENCE

In this paper, we select two main metrics (average acceptance ratio and long-term average revenue to cost ratio) to directly prove the effectiveness and efficiency of VNE-RIA under general interference.
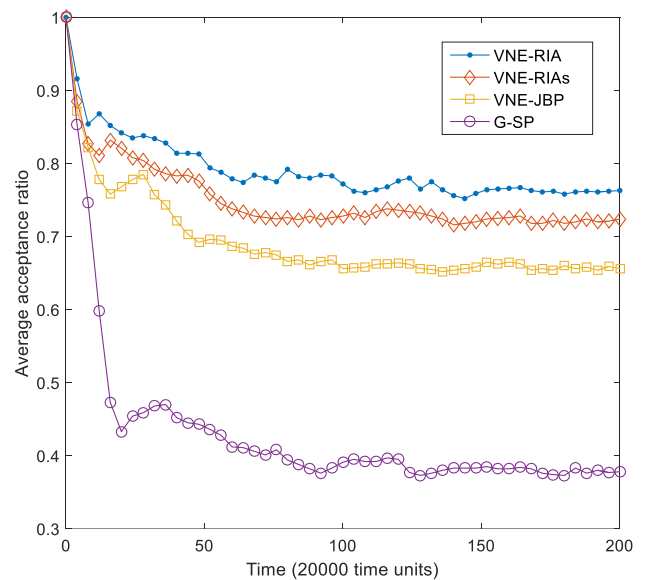

FIGURE 4. Average acceptance ratio.

Fig. 4 illustrates the average acceptance ratios as a function of time for all the selected heuristic embedding algorithms. Observed from the Fig. 4, all algorithms have stable average acceptance ratios since there will exit a balance between substrate network resources and the total number of running ATVN requests (that occupy resources) with the simulation time extending. In addition, our proposed VNE-RIA has the highest stable average acceptance ratio that is closed to be 0.77, outperforming other three selected algorithms. In VNE-RIA, the novel node ranking approach takes the complex

interference into consideration. Through utilizing the total transmission rate as node ranking value, the substrate nodes with relatively higher capacity may be selected for mapping virtual nodes under the complex interference. Also, the link mapping adopts the improved anypath routing scheme which utilizes the link instability for the wireless environment, considering the influence of different transmission rates. A reliable and efficient embedding is therefore more likely to be achieved for one arrived ATVN request. However, VNE-RIAs adopts the multipath link mapping which may not be proper for the unreliable quality of wireless links. Therefore, VNE-RIAs is not able to behave as well as the VNE-RIA algorithm. To the remaining VNE algorithms (G-SP and VNE-JBP), the node mapping does not consider the influence of complex interference on the node ranking value. Also, the complex interference is not fully utilized in the link mapping. Therefore, their average acceptance ratios are relatively lower.
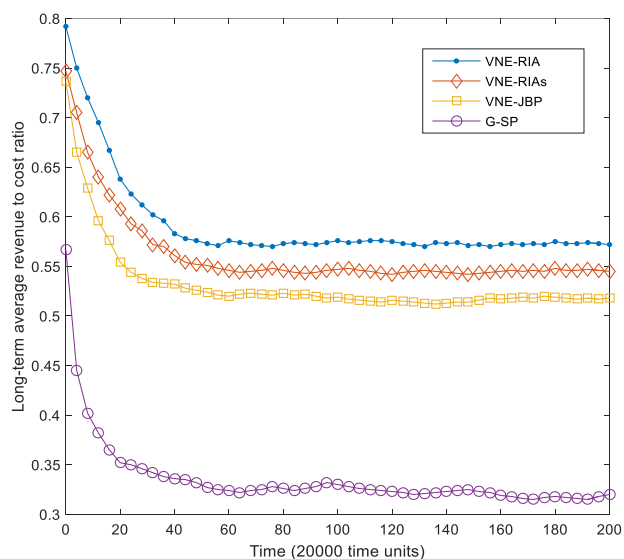

FIGURE 5. Long-term average revenue to cost ratio.

Fig. 5 illustrates the long-term average revenue to cost ratios as a function of time for the four selected VNE algorithms. With the simulation time increasing, the long-term average revenue to cost ratio will decrease to a stable state for all algorithms. To G-SP, it has the lowest long-term average revenue to cost ratio since its average acceptance ratio is the lowest, not fully utilizing substrate network resources. To VNE-JBP, node mapping joints the node power resource and link bandwidth resource to decrease the influence of bottleneck links, saving more required resources than G-SP. However, compared with the VNE-RIAs, VNE-JBP is not able to get better performance. This is expected for consuming too much unnecessary network resources since VNE-JBP does not consider the interference of complex interference in the node mapping as VNE-RIAs does. In addition, VNE-RIA further takes the influence of link interference on link mapping by adopting the improved anypath approach. Through

conducting the simulation, it is apparent that the reliable node mapping and link mapping of VNE-RIA further ensures the efficiency of substrate network resources usage in the long term. It has the highest long-term average revenue to cost ratio that is close to 0.55.

2) COMPARISION UNDER CHANGING INTERFERENCE
Besides the above two metrics, we select the other two metrics (average node utilization and average link utilization) to further prove the effectiveness and efficiency of VNE-RIA under changing interference.
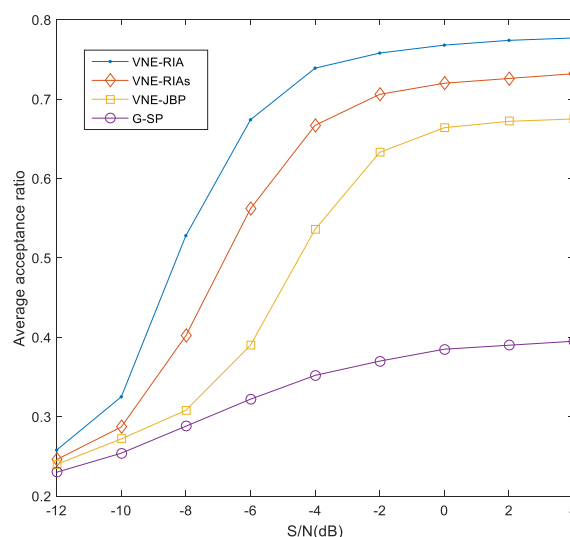

FIGURE 6. Average acceptance ratio.

Fig. 6 illustrates the comparison of average acceptance ratios for the selected four VNE algorithms under changing interference. Derived from the Fig. 6, the average acceptance ratio of all VNE algorithms decreases as the S/N decreases (the effective power of malicious attacks increases). This decay shows it is difficult for the ATVN requests to be mapped as the ATSN suffers from malicious attacks. In addition, our proposed VNE-RIA algorithm outperforms all selected VNE heuristic algorithms since the complex interference is taken into consideration in the node ranking value and link mapping adopts the improved anypath routing scheme for the unstable wireless links in ATSN. It is therefore likely to achieve a more reliable and efficient embedding for the arrived ATVN request. In VNE-RIAs, the node mapping considers the complex interference. However, the link mapping adopts the multipath approach that is not proper for the unstable wireless links. For the next two selected algorithms (VNE-JBP and G-SP), the complex interference is not fully considered in both node mapping and link mapping. Thus, their average acceptance ratios are relatively lower than that of VNE-RIA and VNE-RIAs since less ATVN requests are successfully accepted as the complex interference gets worse.

Fig. 7 illustrates the comparison of long-term average revenue to cost ratios for the selected four VNE algorithms
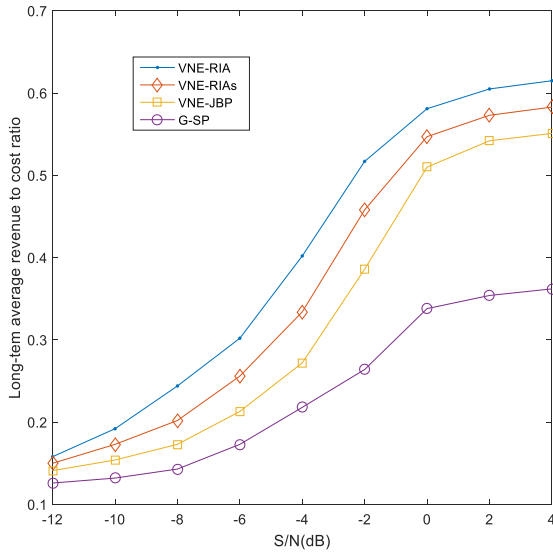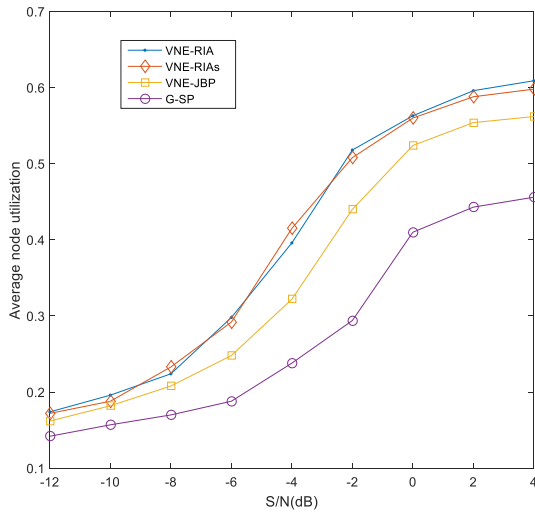
FIGURE 7. Long-term average revenue to cost ratio.
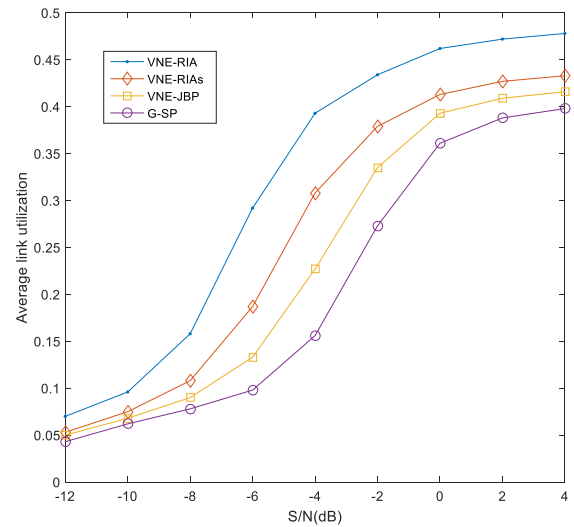

FIGURE 8. Average node utilization.

FIGURE 9. Average link utilization.

Fig. 8 and Fig. 9 illustrate the comparison of average node utilization and link utilization under changing interference, respectively. As the S/N decreases, the curves of average node utilization and link utilization also drop since the node and link resource are not fully utilized as the arrived ATVN requests are rejected under the harsh interference. As shown in Fig. 8, to the node utilization, VNE-RIA and VNE-RIAs have an apparent advantage over the remaining heuristic algorithms since the complex interference is taken into consideration in the node ranking value. As the S/N decreases, more reliable substrate nodes can be selected for mapping virtual nodes. As shown in Fig. 9, to the link utilization, VNE-RIA outperforms other three heuristic algorithms since the improved anypath routing approach is adopted in link mapping and ensures reliable wireless links can be selected in the substrate path for mapping virtual links. The remaining three heuristic algorithms all adopt the shortest path approach in the link mapping and thus perform similarly.

VI. CONCLUSION AND FUTURE NETWORK

To solve the ossification problem of traditional ATNs, a reliable interference-aware algorithm, termed VNE-RIA, is proposed to heuristically embed various airborne tactical virtual networks to contribute to the virtualization for ATNs under the complex interference in air-combat field. Node mapping and link mapping are coordinated to improve the long-term embedding performance. In the node mapping, the interference of link instability and malicious attacks is taken into consideration in the novel node ranking approach to select reliable substrate nodes for mapping virtual nodes under the complex interference of ATNs. In the link mapping, VNE-RIA employs an improved anypath routing approach which can exploit the influence of different transmission rates and the instability of wireless links in the ATNs. Simulation results reveal that VNE-RIA algorithm outperforms typical and state-of-the-art heuristic algorithms for wireless VNE in

under changing interference. As the S/N decreases, the long-term average revenue to cost ratio decreases, which is depicted in Fig. 7. In G-SP, the complex interference is not taken into consideration in node mapping and link mapping. As the S/N decreases, it may consume large amount of unnecessary substrate resource to embed the arrived ATVN request. To VNE-JBP, the complex interference is considered in the link mapping for wireless links. Therefore, it gets a higher long-term average revenue to cost ratio as the S/N decreases. Compared with G-SP and VNE-JBP, VNE-RIAs and VNE-RIA take the influence of complex interference into calculating node ranking value and manage to behave better. In addition, VNE-RIA further adopts the improved anypath routing link mapping, fully exploiting the wireless links in ATSN. Therefore, as the S/N decreases, VNE-RIA saves more extra substrate resource and performs better than VNE-RIAs.

terms of the average acceptance ratio and long-term average revenue to cost ratio under the complex interference.

For the future work, there are still a number of important issues that remain to be completed. First of all, it is to upload the VNE-RIA algorithm in a real testbed environment and evaluate the VNE-RIA algorithm through a prototype implementation. Next, other network dynamics (link failure and node mobility) are needed to be considered to improve the reliability of the proposed VNE-RIA algorithm for embedding ATVNs.

REFERENCES

[1] K. Chen, S. Zhao, N. Lv, W. Gao, X. Wang, and X. Zou, "Segment routing based traffic scheduling for the software-defined airborne backbone network," *IEEE Access*, vol. 7, pp. 106162–106178, Jul. 2019.

[2] J. Wang, P. Deutsch, A. Coyle, T. Shake, and B.-N. Cheng, "An implementation of a flexible topology management system for aerial high capacity directional networks," in *Proc. MILCOM IEEE Mil. Commun. Conf.*, Oct. 2015, pp. 991–996.

[3] A. Tiwari, A. Ganguli, A. Sampath, D. S. Anderson, B.-H. Shen, N. Krishnamurthi, J. Yadegar, M. Gerla, and D. Krzysiak, "Mobility aware routing for the airborne network backbone," in *Proc. MILCOM IEEE Mil. Commun. Conf.*, Nov. 2008, pp. 1–7.

[4] B.-N. Cheng, F. J. Block, B. R. Hamilton, D. Ripplinger, C. Timmerman, L. Veytser, and A. Narula-Tam, "Design considerations for next-generation airborne tactical networks," *IEEE Commun. Mag.*, vol. 52, no. 5, pp. 138–145, May 2014.

[5] A. Kott, A. Swami, and B. J. West, "The Internet of battle things," *Computer*, vol. 49, no. 12, pp. 70–75, Dec. 2016.

[6] N. N. Sapavath and D. B. Rawat, "Wireless virtualization architecture: Wireless networking for Internet of Things," *IEEE Internet Things J.*, vol. 7, no. 7, pp. 5946–5953, Jul. 2020.

[7] C. Liang and F. R. Yu, "Wireless network virtualization: A survey, some research issues and challenges," *IEEE Commun. Surveys Tuts.*, vol. 17, no. 1, pp. 358–380, 1st Quart., 2015.

[8] J. van de Belt, H. Ahmadi, and L. E. Doyle, "Defining and surveying wireless link virtualization and wireless network virtualization," *IEEE Commun. Surveys Tuts.*, vol. 19, no. 3, pp. 1603–1627, 3rd Quart., 2017.

[9] A. Blenk, A. Basta, M. Reisslein, and W. Kellerer, "Survey on network virtualization hypervisors for software defined networking," *IEEE Commun. Surveys Tuts.*, vol. 18, no. 1, pp. 655–685, 1st Quart., 2016.

[10] A. Fischer, J. F. Botero, M. T. Beck, H. de Meer, and X. Hesselbach, "Virtual network embedding: A survey," *IEEE Commun. Surveys Tuts.*, vol. 15, no. 4, pp. 1888–1906, 4th Quart., 2013.

[11] P. Zhang, H. Yao, and Y. Liu, "Virtual network embedding based on computing, network, and storage resource constraints," *IEEE Internet Things J.*, vol. 5, no. 5, pp. 3298–3304, Oct. 2018.

[12] M. Pham, D. B. Hoang, and Z. Chaczko, "Congestion-aware and energy-aware virtual network embedding," *IEEE/ACM Trans. Netw.*, vol. 28, no. 1, pp. 210–223, Feb. 2020.

[13] Y. Su, X. Meng, Q. Kang, and X. Han, "Survivable virtual network link protection method based on network coding and protection circuit," *IEEE Access*, vol. 6, pp. 67477–67493, 2018.

[14] H. Cao, L. Yang, and H. Zhu, "Novel node-ranking approach and multiple topology attributes-based embedding algorithm for single-domain virtual network embedding," *IEEE Internet Things J.*, vol. 5, no. 1, pp. 108–120, Feb. 2018.

[15] M. Li, C. Chen, C. Hua, and X. Guan, "Intelligent latency-aware virtual network embedding for industrial wireless networks," *IEEE Internet Things J.*, vol. 6, no. 5, pp. 7484–7496, Oct. 2019.

[16] O. Kaiwartya, A. H. Abdullah, Y. Cao, J. Lloret, S. Kumar, R. R. Shah, M. Prasad, and S. Prakash, "Virtualization in wireless sensor networks: Fault tolerant embedding for Internet of Things," *IEEE Internet Things J.*, vol. 5, no. 2, pp. 571–580, Apr. 2018.

[17] S. Abdelwahab, B. Hamdaoui, M. Guizani, and T. Znati, "Efficient virtual network embedding with backtrack avoidance for dynamic wireless networks," *IEEE Trans. Wireless Commun.*, vol. 15, no. 4, pp. 2669–2683, Apr. 2016.

[18] D. Yun, J. Ok, B. Shin, S. Park, and Y. Yi, "Embedding of virtual network requests over static wireless multihop networks," *Comput. Netw.*, vol. 57, no. 5, pp. 1139–1152, Apr. 2013.

[19] P. Lv, X. Wang, and M. Xu, "Virtual access network embedding in wireless mesh networks," *Ad Hoc Netw.*, vol. 10, no. 7, pp. 1362–1378, Sep. 2012.

[20] G. Chochlidakis and V. Friderikos, "Mobility aware virtual network embedding," *IEEE Trans. Mobile Comput.*, vol. 16, no. 5, pp. 1343–1356, May 2017.

[21] N. Pathak, S. Misra, A. Mukherjee, A. Roy, and A. Y. Zomaya, "UAV virtualization for enabling heterogeneous and persistent UAV-as-a-Service," *IEEE Trans. Veh. Technol.*, vol. 69, no. 6, pp. 6731–6738, Jun. 2020.

[22] H. Cao, H. Hu, Z. Qu, and L. Yang, "Heuristic solutions of virtual network embedding: A survey," *China Commun.*, vol. 15, no. 3, pp. 186–219, Mar. 2018.

[23] J. Lischka and H. Karl, "A virtual network mapping algorithm based on subgraph isomorphism detection," in *Proc. 1st ACM Workshop Virtualized Infrastruct. Syst. Archit. - VISA*, Jan. 2009, pp. 81–88.

[24] L. Gong, Y. Wen, Z. Zhu, and T. Lee, "Revenue-driven virtual network embedding based on global resource information," in *Proc. IEEE Global Commun. Conf. (GLOBECOM)*, Dec. 2013, pp. 2294–2299.

[25] L. Gong, H. Jiang, Y. Wang, and Z. Zhu, "Novel location-constrained virtual network embedding LC-VNE algorithms towards integrated node and link mapping," *IEEE/ACM Trans. Netw.*, vol. 24, no. 6, pp. 3648–3661, Dec. 2016.

[26] T. H. Cormen, C. Stein, R. Rivest and C. Leiserson, *Introduction to Algorithms*, 2nd ed. New York, NY, USA: McGraw-Hill, 2001.

[27] M. Yu, Y. Yi, J. Rexford, and M. Chiang, "Rethinking virtual network embedding: Substrate support for path splitting and migration," *ACM SIGCOMM Comput. Commun. Rev.*, vol. 38, no. 2, pp. 17–29, Mar. 2008.

[28] B. Cao, S. Xia, F. He, and Y. Yi, "Research of embedding algorithm for wireless network virtualization," *J. Commun.*, vol. 1, no. 38, pp. 35–43, Jan. 2017.

[29] M. Li, C. Hua, C. Chen, and X. Guan, "Application-driven virtual network embedding for industrial wireless sensor networks," in *Proc. IEEE Int. Conf. Commun. (ICC)*, May 2017, pp. 1–6.

[30] K. Chen, N. Lv, S. Zhao, X. Wang, and J. Zhao, "A scheme for improving the communications efficiency between the control plane and data plane of the SDN-enabled airborne tactical network," *IEEE Access*, vol. 6, pp. 37286–37301, 2018.

[31] I. Khan, F. Belqasmi, R. Glitho, N. Crespi, M. Morrow, and P. Polakos, "Wireless sensor network virtualization: A survey," *IEEE Commun. Surveys Tuts.*, vol. 18, no. 1, pp. 553–576, 1st Quart., 2016.

[32] R. Laufer, H. Dubois-Ferriere, and L. Kleinrock, "Multirate anypath routing in wireless mesh networks," in *Proc. IEEE INFOCOM 28th Conf. Comput. Commun.*, Apr. 2009, pp. 37–45.

[33] H. Cao, H. Zhu, and L. Yang, "Collaborative attributes and resources for single-stage virtual network mapping in network virtualization," *J. Commun. Netw.*, vol. 22, no. 1, pp. 61–71, Feb. 2020.

JINGCHENG MIAO received the B.S. degree in telecommunication engineering and the M.S. degree in signal and information processing from the Engineering University of PAP, Xi'an, China, in 2016 and 2018, respectively. He is currently pursuing the Ph.D. degree in aerospace network with Air Force Engineering University, Xi'an.

His research interests include airborne tactical networks, network virtualization, and virtual network embedding.

NA LV received the B.S. degree in testing technology and instrumentation, the M.S. degree in control theory and applications, and the Ph.D. degree in armament science and technology from Northwestern Polytechnical University (NWPU), Xi'an, China, in 1992, 1995, and 2010, respectively.

She is currently a Full Professor with the Air Force Engineering University, Xi'an. Her current research interests include aviation data link systems, military air communications, and software-defined networking.

WEITING GAO received the B.S., M.S., and Ph.D. degrees in communication and information system from Northwestern Polytechnical University (NWPU), Xi'an, China, in 2007, 2011, and 2015, respectively.

He is currently a Lecturer with Air Force Engineering University, Xi'an. His research interests include airborne networks and communication system design.

KEFAN CHEN received the B.S. degree from the University of Electronic Science and Technology of China (UESTC), Chengdu, China, in 2013, and the M.S. and Ph.D. degrees from Air Force Engineering University, Xi'an, China, in 2016 and 2019, respectively.

He is currently an Engineer. His research interests include airborne tactical networks, software-defined networking, and aviation data link.
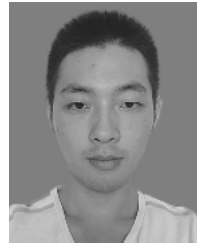
YANHUI ZHANG received the B.S. degree in telecommunication engineering from Air Force Engineering University, Xi'an, China, where he is currently pursuing the M.S. degree in communication and information system.

His research interests include software-defined networking, machine learning, and military aviation communication.

• • •